MEASUREMENTS OF FREQUENCIES OF SOLAR OSCILLATIONS FROM THE MDI MEDIUM-l PROGRAM

E.J. RHODES, JR.
Department of Physics and Astronomy, University of Southern California, Los Angeles, CA 90089, and Space Physics Research Element, Jet Propulsion Laboratory, Pasadena, CA 91101, USA

A.G. KOSOVICHEV, J. SCHOU and P.H. SCHERRER
W.W. Hansen Experimental Physics Laboratory, Stanford University, Stanford, CA 94305, USA

J. REITER
Mathematisches Institut, Technische Universität München, D-80333 Munich, Germany

Abstract. Inversions of solar internal structure employ both the frequencies and the associated uncertainties of the solar oscillation modes as input parameters. In this paper we investigate how systematic errors in these input parameters may affect the resulting inferences of the sun's internal structure. Such systematic errors are likely to arise from inaccuracies in the theoretical models which are used to represent the spectral lines in the observational power spectra, from line blending, from asymmetries in the profiles of these lines, and from other factors. In order to study such systematic effects we have employed two different duration observing runs (one of 60 days and the second of 144 days) obtained with the Medium-l Program of the Michelson Doppler Imager experiment onboard the SOHO spacecraft. This observing program provides continuous observations of solar oscillation modes having angular degrees, l, ranging from 0 to $\sim$ 300. For this study intermediate- and high-degree p-mode oscillations having degrees less than 251 were employed.

In the first of our tests we employed two different methods of estimating the modal frequencies and their associated uncertainties from the 144-day observational power spectra. In our second test we also repeated both methods of frequency estimation on the 60-day time series in order to assess the influence of the duration of the observed time series on the computed frequencies and uncertainties. In a third test we investigated the sensitivity of the computed frequencies to the choice of initial-guess, or "seed" frequencies that are used in the frequency estimation codes. In a fourth test we attempted to investigate the possible systematic frequency errors which are introduced when the observational asymmetry in the p-mode peaks is ignored. We carried out this particular test by fitting simple models of asymmetric line profiles to the peaks in the observational power spectra. We were then able to compute the differences between those frequencies and our previous frequencies which had been obtained using the assumption that all of the observational peaks were symmetric in shape.

In order to study the possible influence of the two different frequency estimation methods upon the radial profile of the internal sound speed, we carried out four parallel structural inversions using the different sets and subsets of frequency estimates and uncertainties as computed from the 144-day observing run as inputs. The results of these four inversions confirm the previous finding by the GONG project (Gough *et al.*, 1996) and by the MDI Medium-l Program (Kosovichev *et al.*, 1997) that, in a thin layer just beneath the convection zone, helium appears to be less abundant than predicted by theory. However, differences in our four inverted radial sound speed profiles demonstrate that the currently-available techniques for determining the frequencies of the Medium-l oscillation peaks introduce systematic errors which are large enough to affect the results of the structural inversions. Moreover, based upon the differences in these four inverted sound speed profiles, it appears that the choice of which subset of modes is included in a particular inversion and which modes are not included may also be introducing systematic errors into our

current understanding of solar internal structure. Hence, it appears to be very important that consistent sets of modal selection criteria be employed.

Finally, at least one of the two frequency estimation codes which we used was not sensitive to changes in the input "seed" frequencies which were employed as initial guesses for that code. This result allays fears that the difference in the helium abundance between the sun and the reference solar model in the thin layer beneath the convection zone which was mentioned above might have been due to the particular seed frequencies which were employed in the earlier inversions. Since this thin layer may likely be the place where the solar dynamo operates, it will be extremely important to observe any possible evolution of this transition layer throughout the upcoming 11-year activity cycle.

1. Introduction

The two principal goals of helioseismology are: 1) the inference of the thermodynamic structure and 2) the inference of the dynamical motions of the solar interior as functions of both position within the Sun and of time. The principal means by which both of these goals are now being sought is the inversion of the observed properties of the solar normal modes of oscillation. In the case of the thermodynamic structure it is the oscillation frequencies themselves (weighted by their uncertainties) which are the input data for the inversions, while in the case of the dynamical motions it is the frequency splittings (again properly weighted) which are inverted. As is described elsewhere (Kosovichev et al., 1997), it is only the frequencies and splittings of the solar f- and p-mode oscillations have been inverted until now. Because of the stochastic nature of solar oscillations (illustrated in the solar sounds files on the CD-ROM), one of the most important and difficult problems in the frequency measurements is how to account for the stochastic component in the oscillation spectra. In this paper, we discuss two different spectral fitting procedures: the so-called mean-multiplet and averaged-spectra techniques.

Our main goal in this paper is to demonstrate how these two different fitting techniques, which we have employed to estimate the frequencies of the normal modes from the MDI Medium-l data, may influence the inferred radial profile of the solar internal sound speed. Our additional goals are: 1)to learn how the frequencies and uncertainties depend upon the duration of the observing run from which they are computed, 2)to learn how the asymmetry which is present in the observational power spectra will alter the frequencies which are obtained under the assumption of symmetric shapes for those peaks, 3)to learn whether or not the frequencies which have been computed might be sensitive to changes in the initial guesses which are employed in the frequency estimation programs, and 4) to study the effects of modal selection critera upon the inverted results.

For all of these tests we have employed observations which were obtained by the Solar Oscillation Investigation/ Michelson Doppler Imager (SOI/MDI) experiment on board the Solar and Heliospheric Observatory (SOHO) spacecraft. In particular, we have employed time series of oscillation observations which were made with the

MDI Medium-l Program. This program has been described in detail by Scherrer et al. (1996).

In Section 2 we will describe the different MDI observing runs which we employed in our study. In Section 3 we will describe the two different methods which we employed in the estimation of the intermediate-l frequencies from these observing runs. We will also describe in this section how we evaluated the effects of the observational asymmetry in the observed power spectral peaks upon the frequency estimates. Next we will describe how two different sets of "seed" frequencies were employed as input parameters for one of the two different frequency estimation programs.

The inferred radial profiles of the solar internal sound speed which resulted from the different inversions we carried out will be presented in Section 4, while in Section 5 we will discuss the relative importance of all of these different effects upon the resulting sound speed profiles.

2. The MDI Medium-l Observations

As described by Scherrer et al. (1996) the Medium-l Program of the SOI/MDI experiment is dedicated to the nearly-continuous monitoring of the Doppler velocity field of the visible solar hemisphere. The Medium-l data are transmitted though the low-rate (5 kbps) telemetry channel of SOHO. It is this relatively low bit rate which limits the spatial resolution of the Medium-l observations. This low data rate also requires that some initial processing of the original 1024×1024-pixel CCD full-disk Dopplergrams be carried out on board the MDI instrument. Specifically, for both Medium-l observing runs which we employed in this study, the Dopplergrams were binned with Gaussian weights on a square 5×5-pixel grid. The binned images which resulted from this procedure were then generated on board the spacecraft once per minute. With the exception of rare instrumental problems and occasional telemetry drop outs these binned Doppler maps were then transmitted to the earth on a minute-by-minute basis.

The first of the two Medium-l observing runs which we employed was obtained on 60 consecutive days running from May 25, 1996, through July 24, 1996. The overall duty cycle of this run was 0.9801. The second of the two runs we used covered a span of 144 days which ran from May 9, 1996, through September 29, 1996. The overall duty cycle of this run was 0.9547 (see a 5-hour movie of the time series on the CD-ROM). A autoregressive gap-filling technique, Brown(1996), was employed to fill-in relatively short gaps in the time series generated from the second run and its overall duty cycle was raised to 0.9639. As can be noted from the dates given above these two data sets were not independent of each other. Rather, the shorter-duration run is a sub-set of the longer run. This choice of time intervals was made in order to minimize the possible influence of any solar-cycle dependent frequency shifts on our study.

3. Analysis of the Medium-l Data

3.1. Power Spectra

The procedures which we employed to convert the time series of Medium-l observations into power spectra are described in Kosovichev et al. (1997) in this volume. For both the 60-day and 144-day observing runs we computed power spectra for all $2l+1$ individual m-values at every degree ranging from $l=0$ through $l=299$. Hence, for every non-zero degree greater than two, each set of power spectra consisted of one zonal (i.e. $l=0$), two sectoral (i.e., $m=-l$ and $m=+l$), and $2l-2$ tesseral (i.e., l not equal to m for non-zero m) power spectra. The spectra which were computed from the 60-day observing run contained 43,201 points each. The spectra computed from the 144-day run contained 103,680 points each. The formal frequency resolution of the 43,201-point power spectra was 0.192901 μHz, while the resolution of the 103,680-point spectra was 0.0803755 μHz.

In addition to these two complete sets of power spectra, we also computed two sets of m-averaged power spectra. In the procedure, which collapsed each set of spectra into a single averaged spectrum, we approximated the frequency splitting which is introduced into each multiplet of modes by the solar internal rotation and asphericity with a polynomial expansion similar to that of Duvall, Harvey, and Pomerantz (1986):

$$\nu_{nlm} = \nu_{nl} + \sum_{k=1}^{36} a_{nl}^{(k)} \mathcal{P}_k^{(l)}(m), \tag{1}$$

where ν_{nl} is the mean frequency of a mode multiplet, and $\mathcal{P}_k^{(l)}(m)$ are orthogonal polynomials of degree k defined by

$$\mathcal{P}_k^{(l)}(l) = l, \quad \text{and} \quad \sum_{m=-l}^{l} \mathcal{P}_i^{(l)}(m)\mathcal{P}_j^{(l)}(m) = 0 \quad \text{for} \quad i \neq j. \tag{2}$$

The polynomials, $\mathcal{P}_k^{(l)}(m)$, can be expressed in terms of the Clebsch-Gordan coefficients (Ritzwoller and Lavely, 1991). At $l >> k$, $\mathcal{P}_i^{(l)}(m) \rightarrow LP_k(m/L)$, where $L = l + 1/2$, and P_k are the Legendre polynomials. In this limit, coefficients, $a_{nl}^{(k)}$ are equivalent to the coefficients introduced by Duvall, Harvey, and Pomerantz (1986). Since

$$\sum_{m=-l}^{l} \mathcal{P}_k^{(l)}(m) = 0 \quad \text{for} \quad k > 0, \tag{3}$$

the mean frequencies, ν_{nl}, depend only on the spherically symmetric component of the solar structure. Frequency splitting coefficients, $a_{nl}^{(k)}$, for even k depend on the aspherical component of the structure, while the coefficients for odd k measure the rotation rate (*e.g.* Gough, 1993). Therefore, in the method in which we collapsed

the individual power spectra into m-averaged spectra we wanted to remove the effects of solar rotation from the individual spectra and to accomplish this goal we used non-zero values for the three odd-k splitting coefficients (i.e., $a_{nl}^{(1)}$, $a_{nl}^{(3)}$, and $a_{nl}^{(5)}$). In particular, the three even-k splitting coefficients (i.e., $a_{nl}^{(0)}$, $a_{nl}^{(2)}$, and $a_{nl}^{(4)}$) were each set equal to zero because they were each extremely small in comparison with the three odd-k coefficients. Also, no higher-k coefficients were included in the expansion because they were all very small in magnitude in comparison with the three coefficients which were employed.. Finally, in the procedure which averaged together the shifted tesseral power spectra, we used a single frequency shift for each separate tesseral or sectoral spectrum. We did not apply a separate frequency shift for each multiplet within that spectrum. The $2l$ shifted spectra were then averaged together with the unshifted zonal spectrum. In this procedure each of the separate spectra was included with equal weight. No attempt was made to weight each separate spectrum according to its m-value. The 301 m-averaged power spectra are shown as a two-dimensional l-ν diagram on the CD-ROM (Fig.1b).

3.2. Frequency Estimation Techniques

3.2.1. *Mean-Multiplet Technique*

The first of our two different frequency estimation techniques was the so-called "mean-multiplet" technique of Schou(1992). In this technique the power spectral peaks are assumed to have a symmetric Lorentzian shape and a maximum likelihood method is employed to determine the parameters of Lorentzian profiles. Furthermore, in this method the peaks are fit simultaneously in all of the $2l+1$ individual power spectra for each multiplet so that the effects of overlapping peaks can be included in the fits. These $2l+1$ frequencies are then averaged to yield a single frequency, ν_{nl}, for that multiplet. In addition, an associated frequency uncertainty, σ_{nl}, and a set of frequency splitting coefficients, $a_{nl}^{(k)}$, for which k runs from 1 to 36, are obtained for the same multiplet. The mean frequencies which resulted from the use of this technique on the power spectra from the 144-day MDI Medium-l observing run were illustrated in Figure 11 of Kosovichev et al. (1997).

3.2.2. *Averaged-Spectrum Technique*

The second frequency estimation technique which we employed has recently been described by Reiter and Rhodes(1997). This technique is an elaboration and refinement of the least-squares fitting technique employed earlier by Korzennik (1990) in the analysis of data obtained with the Mt. Wilson Observatory's 60-Foot Solar Tower. This technique is becoming known as the "averaged-spectrum" method because it employs the m-averaged power spectra rather than the $2l+1$ individual power spectra which the mean-multiplet method employs.

The application of this second technique results in a single frequency for each multiplet rather than a set of $2l+1$ frequencies which must later be averaged

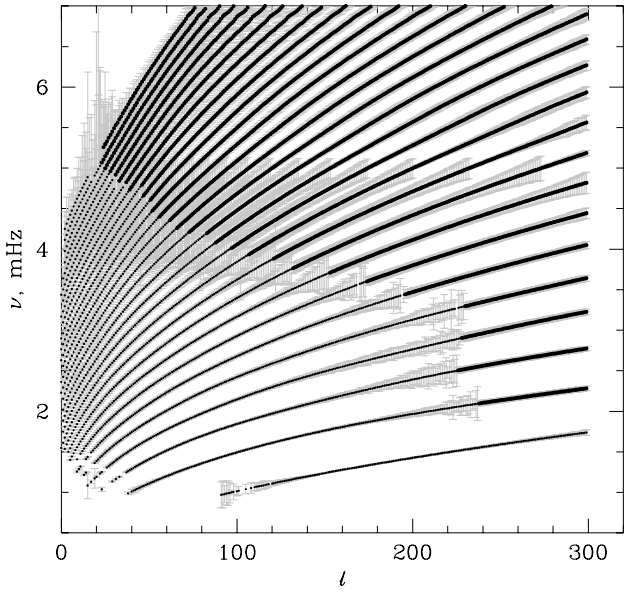

Figure 1. Multiplet frequencies determined from m-averaged power spectra obtained from the MDI 144-Day Observing Run using the averaged-spectrum method are shown as the small dots. Ridge-fit frequencies determined with the averaged-spectrum method as applied to entire p-mode ridges rather than individual modal peaks are shown as the larger dots along the extensions of the ridges toward higher degrees and frequencies. The formal frequency uncertainties obtained from the averaged-spectrum method are superimposed upon both the modal and ridge-fit frequencies in gray. For frequencies below 5000 μHz the frequency uncertainties of the modal fits were multiplied by a factor of 1000 before being plotted. For frequencies greater than 5000 μHz the uncertainties of the ridge fits were divided by 10 instead. The uncertainties of the ridge fits below 5000 μHz were not modified. A color version of this figure (Fig.1a) is on the CD-ROM. In Figure 1a the modal-fit frequencies are shown in blue, the ridge-fits are shown in red, and both sets of uncertainties are shown in yellow. Figure 1a may be compared with the m-averaged spectrum (Fig.1b) on the CD-ROM. Samples of the MDI full-disk (Fig.1c) and medium-l Dopplergrams (Fig.1d) are also shown on the CD-ROM.

together to yield an estimate of the average multiplet frequency. (We note here that the mean-multiplet technique includes includes fits to several of the spatial sidelobes which are located on both sides of each true peak within a given multiplet. Hence, this technique fits many more peaks in its estimation of multiplet frequencies than does the averaged-spectrum technique.)

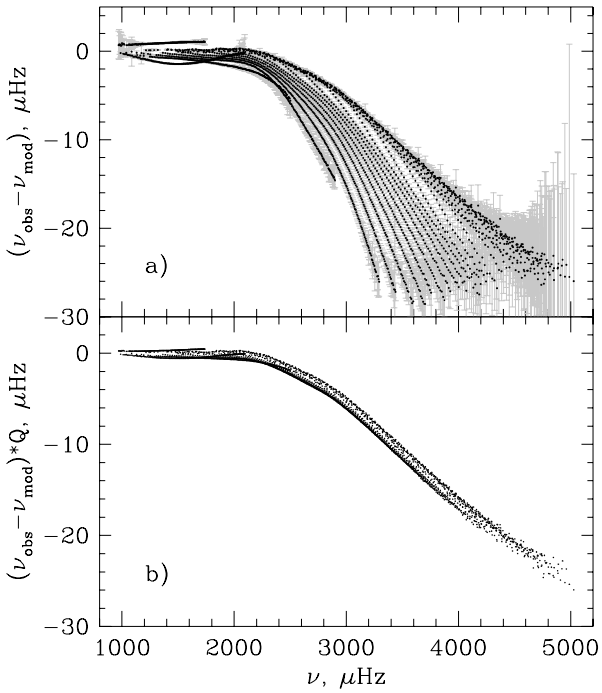

Figure 2. a) Frequency dependence of differences between averaged-spectrum frequency estimates and reference solar model frequencies (the frequency uncertainties were multiplied by a factor of 10 before being plotted in gray): b) The same frequency differences scaled with mode inertia Q.

3.3. Averaged-Spectrum Results

The coverage in the l-ν plane which resulted from the application of the averaged-spectrum fitting technique to the set of m-averaged power spectra computed from the 144-day observing run is shown here in Figure 1. We note that there were only a small number of spectral peaks for which we were able to obtain a converged fit in the spectrum computed from the 144-day run but for which we were unable to obtain a corresponding converged fit in the 60-day spectrum.

In addition to the 2794 modal frequencies which are shown in Figure 1 as the small dots (and which are shown in blue in the color version of this Figure on the CD-ROM), we have also included in this figure an additional 4555 so-called "ridge-fit" frequency estimates which are shown as the larger dots (and which are

shown in red on the CD-ROM). These ridge-fit frequency estimates were obtained from the application of the averaged-spectrum method to the entire f- and p-mode ridges instead of to individual modes as was done for the modal fits. Such ridges arise when the spatial sidelobes which occur for several successive degrees overlap so closely in frequency that individual modes can no longer be individually identified. The analysis of such ridge-fit frequencies is now in progress. The results of that analysis will be presented in a future paper.

3.4. Comparison of Frequency Datasets

3.4.1. *Comparison with Reference Solar Model*

The tables of both sets of modal frequencies and their associated frequency uncertainties are presented on the CD-ROM. Once we had generated both frequency estimate datasets, we then compared both of them with a set of theoretical frequencies computed from a reference solar model. The solar model which we chose to use was Model S of Christensen-Dalsgaard et al.(1996). This model was a standard evolutionary model computed using the most recent information on nuclear reaction rates (Bahcall and Pinsonneault, 1995) and radiative opacity and the equation of state (Rogers and Iglesias, 1996). The gravitational settling and diffusion of helium and heavier elements were taken into account in the computation of this model following the theory by Michaud and Proffitt (1993).

The comparison of the observed frequency estimates obtained from the averaged-spectrum method with the theoretical model frequencies is shown here in Figure 2. The raw frequency differences (in the sense of the observed minus the theoretical frequency estimates) are shown as a function of frequency in Figure 2a. We have also included the frequency uncertainties in Figure 2a; however, in order to make them visible at the scale of the figure, we have multiplied these uncertainties by a factor of 10 prior to plotting them. We show a similar comparison between the averaged-spectrum estimates and the theoretical model frequency estimates in which we have normalized the frequency differences by the inertia of the different p-modes in Figure 2b. Once again the frequency uncertainties have been multiplied by a factor of 10 prior to their inclusion in Figure 2b. We have not included a separate pair of plots for the mean-multiplet frequency estimates in Figure 2 as the differences between them and the averaged-spectrum estimates were small enough that they were indistinguishable at the scale of the figure.

3.4.2. *Inter-comparison of 144-Day Observational Frequency Estimates*

In addition to comparing both sets of observed frequency estimates with theoretical frequencies, we also inter-compared the two sets of observational frequency estimates directly. We obtained a total of 1940 different modes for which converged solutions were found for both of our two frequency estimation programs. The differences in the two sets of frequency estimates obtained from the 144-day observing run are shown here in Figure 3. The frequency dependence of the raw frequency

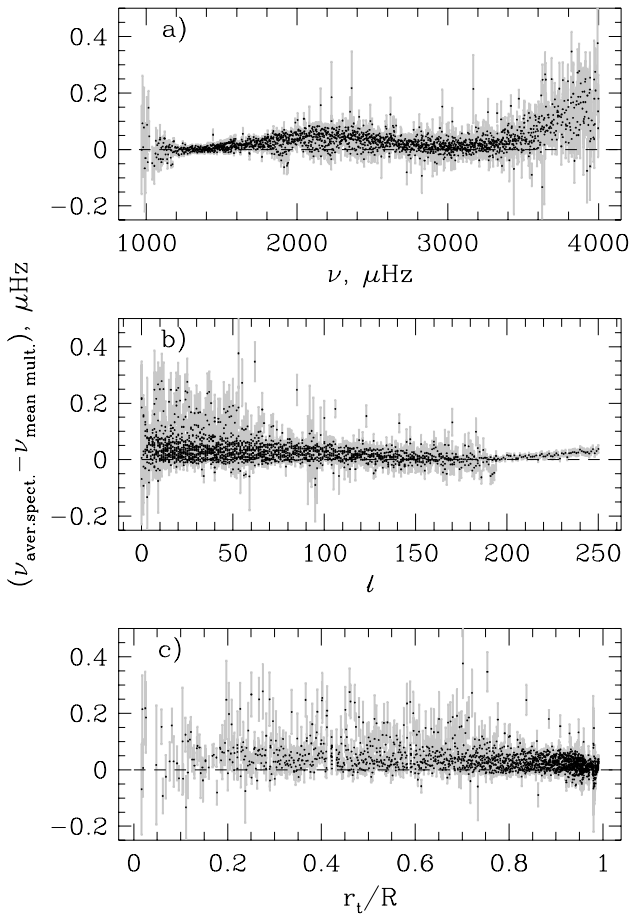

Figure 3. a) Frequency dependence of differences between averaged-spectrum and mean-multiplet frequency estimates: b) The degree dependence of the same frequency differences: c) The dependence of the frequency differences upon the inner turning point radius of the corresponding p-modes. The unscaled frequency uncertainties have been added to all three panels in gray.

differences (in the sense of the averaged-spectrum set minus the mean-multiplet set) are shown in Figure 3a, where we have added the unscaled one-sigma frequency uncertainties. The degree dependence of the same frequency differences is shown in Figure 3b (again with one-sigma errors superimposed). The inner turning

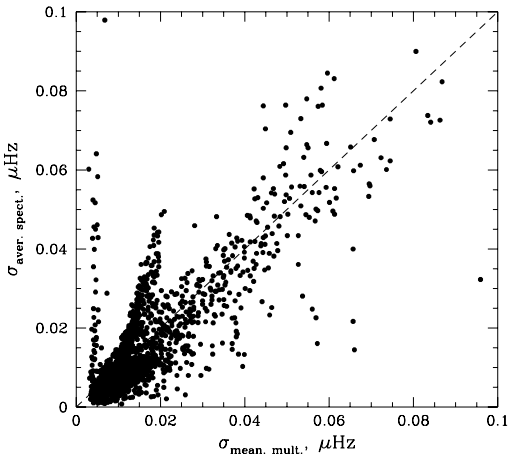

Figure 4. Comparison of 1σ frequency uncertainties inferred from mean-multiplet and averaged-spectrum methods. Most of the points scatter around the diagonal of the figure. This concentration of points shows that in the large majority of cases the two uncertainties are nearly equal.

point dependence of these frequency differences is shown in Figure 3c. It should be noted that the vertical scale of Figure 3 is much smaller than was the scale used in Figure 2. Nevertheless, Figure 3 still shows that there were small, but significant differences in the frequency dependence of the two frequency datasets. The largest differences between the two datasets can be seen at frequencies near 2400 and 3400 μHz. All three panels of Figure 3 illustrate that the averaged-spectrum frequency estimates tended to be larger than those determined from the mean-multiplet method.

Figure 3c also illustrates that the two sets of frequency estimates agreed most closely for modes with inner turning points near the solar surface (i.e., where the fractional radii of the inner turning points are close to unity), and for modes having deep inner turning points (e.g. for modes having inner turning point radii near $0.2R$). For modes having inner turning point radii located in between these two extremes the differences in the two sets of frequencies were larger. The largest frequency differences can be seen to have occured for modes having inner turning point radii near $0.5R$.

In addition to comparing the two sets of frequency estimates from our two different methods, we also compared the estimated frequency uncertainties. The comparison that we made of these uncertainties (also referred to as frequency errors) is shown here in Figure 4. In this figure the uncertainties we obtained from the averaged-spectrum method are plotted as a function of the corresponding uncertainties for the same modes as determined by the mean-multiplet method.

It is evident in Figure 4 that most of the uncertainties were very similar in size; however, there was one group of points which fell near the vertical axis of the figure. These points corresponded to cases in which the uncertainties were considerably larger in the averaged-spectrum method than they were in the mean-multiplet method. This may have been due to the wider peaks in some of the averaged spectra in comparison with the narrower peaks in the unaveraged tesseral power spectra which were used in the mean-multiplet method. The larger uncertainties of these few averaged-spectrum frequency estimates meant that they were assigned less weight in the inversions than were the corresponding mean-multiplet estimates. Fortunately, there were relatively few such cases.

3.5. Comparison of 60-Day and 144-Day Frequency Estimates

The effects of changes in the duration of the observing run from which the power spectra are computed are illustrated here in Figures 5 and 6. The frequency dependence of the differences in two sets of averaged-spectrum frequencies which were computed from the 144-day and from the 60-day MDI Medium-l observing runs is shown in Figure 5a, while the frequency dependence of the differences in the two sets of mean-multiplet frequencies is shown in Figure 5b. Figure 5a indicates that the frequency estimates computed from the averaged-spectrum method do not show any systematic shift between the 144- and 60-day observing runs. In contrast, Figure 5b shows that there was a systematic frequency variation in the two sets of frequencies which were computed using the mean-multiplet method. We note that the frequency variation shown in Figure 5b is very similar in shape to that shown in Figure 3a. It is not at all clear why the frequencies computed from one of our two methods would depend upon the duration of the observing run when those computed from the other method show no such variation. We plan to investigate this issue in the future.

An increase in the duration of the observing run from which the modal parameters are estimated would be expected to result in a decrease in the measured widths of the power spectral peaks and also in a corresponding decrease in the magnitudes of the formal frequency uncertainties of the modes. In order to determine whether or not such expectations were realized during the MDI Medium-l observing program, we also computed the full-width at half maximum (FWHM) of the different power spectral peaks in the two sets of averaged power spectra. We then computed the ratios of the FHWM values computed from the 144-day and 60-day observing runs. When we examined these FWHM ratios, we found that most of these FWHM ratios were indeed less than unity, as was expected.

In a similar fashion we also computed the ratios of the formal frequency uncertainties which resulted from the fits to our two sets of averaged power spectra. The frequency dependence of the ratios in the frequency uncertainties is shown here in Figure 6. The average ratio of the 144-day and 60-day frequency uncertainties was equal to 0.669. Since the frequency uncertainties are expected to scale with

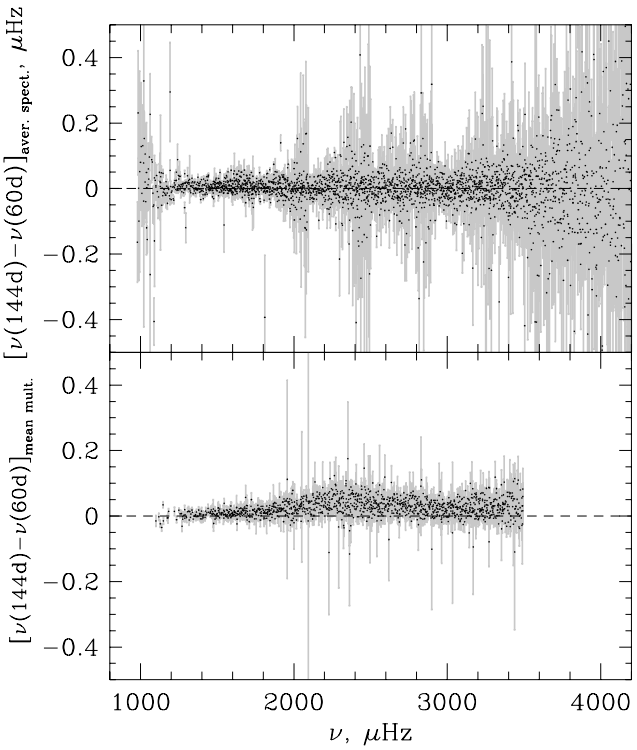

Figure 5. a) Frequency dependence of frequency differences as determined by the averaged-spectrum method applied to power spectra computed from the 144- and 60-day observing runs: b) Frequency dependence of the frequency differences obtained by the mean-multiplet method applied to the same two observing runs. The unscaled frequency uncertainties are superimposed upon both sets of frequency differences in gray.

the square root of the duration of the time series from which they are computed, we would have anticipated the ratio of the 144-day and 60-day uncertainties to be equal to 0.646. The close agreement of the above two numbers does indeed suggest that the frequency uncertainties scale as predicted as the duration of the observing run is increased. We plan to test this scaling of the uncertainties again in the near future when Medium-l power spectra are available for a much longer 360-day observing run.

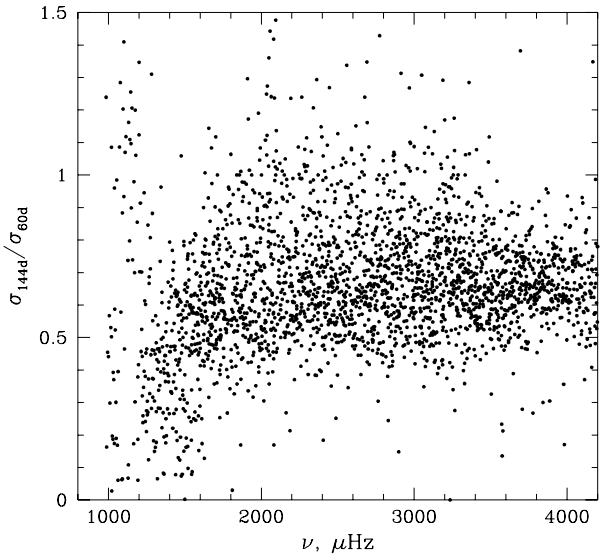

Figure 6. Frequency dependence of the ratios of the frequency uncertainties as computed using the averaged-spectrum method for both the 144- and 60-day observing runs. The ratios of these uncertainties are almost all less than unity and the average ratio was 0.669. Based upon the durations of these two runs the average ratio would be expected to be equal to 0.646.

3.6. Frequency Effects of Asymmetric Power Peaks

Because of the significant reduction in the noise, the Medium-l data have revealed interesting characteristics of the line profiles of the oscillation power spectra. The most interesting feature is the asymmetry of the line profiles. Though the asymmetry has been noticed in the ground-based data (Duvall *et al.*, 1993), frequencies of solar modes are usually determined by assuming that the line profile is symmetric and can be fitted by a Lorentzian, which would be the case if the solar p modes were damped simple harmonic oscillators excited by a stochastic source. However, this leads to systematic errors in the determination of frequencies (Hill *et al.*, 1996; Abrams and Kumar, 1996). Several authors have studied this problem theoretically and have found that there is an inherent asymmetry whenever the waves are excited by a localized source (Gabriel, 1992, 1993, and 1995; Kumar *et al.* 1994; Roxbourgh and Vorontsov, 1995). Physically, the asymmetry is an effect of interference between an outward direct wave from the source and a corresponding inward wave that passes through the region of wave propagation (Duvall *et al.*, 1993). Figure 10 of Kosovichev et al. (1997) shows a theoretical power spectrum

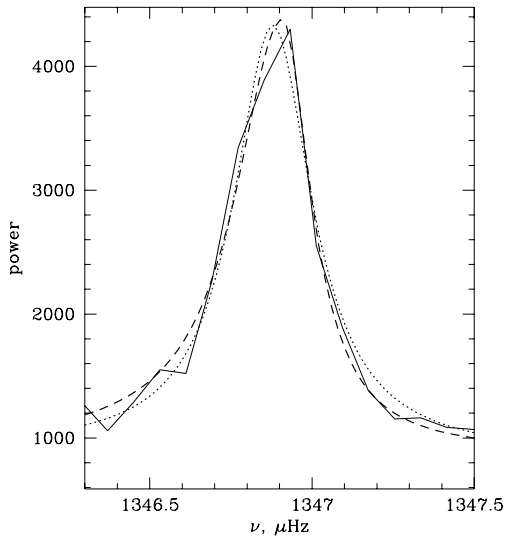

Figure 7. Comparison of observed peak from m-averaged power spectrum obtained from 144-day observing run for $l = 178$, $n = 0$ (solid line) and the numerical fits to this peak computed from the averaged-spectrum method assuming a symmetric fit (dotted line) and assuming an asymmetric Lorentzian profile (dashed line).

of p modes of $l = 200$ obtained by Nigam and Kosovichev (1996). This theoretical model is in good qualitative agreement with the observations. The degree of the asymmetry depends on the relative locations of the acoustic sources and the upper reflection layer of the modes.

An example of an asymmetric peak in the 144-day averaged spectrum is shown as the solid line in Figure 7. The peak shown in this figure is the $l = 178$, $n = 0$ peak. Also shown in this figure are two fitted profiles for this peak. The dotted line is the fit of a symmetric Lorentzian with a linear background term, while the dashed line is the fit of an asymmetric Lorentzian profile in which the two different halves of the profile are both Lorentzian half-profiles each having different half-widths at half-maximum and different amplitudes above the background. The differences between the asymmetric and asymmetric fits are apparent even at the scale of Figure 7. In particular, the peaks of the two different fitted functions are located at different frequencies.

In order to make initial estimates of the errors introduced into the frequency estimates due to the presence of asymmetric peak profiles, we modified the numerical algorithm used in the average-spectrum frequency estimation program to fit four different-shaped profiles to all of the observed peaks in our 144-day spectra.

We then ran this modified version of the program and for each observed peak we selected the model fit which minimized the residuals about that fit as the "best" model for that peak. The first of these four different models was our original symmetric Lorentzian profile with a linearly-varying background. The second model was an asymmetric Lorentzian with linearly-varying background of the type shown in Figure 7. The third model was an asymmetric Lorentzian with a quadratically-varying background and the fourth model was an asymmetric Gaussian with a quadratic background.

The results of running this modified averaged-spectrum program on the 144-day spectra are shown in Figure 8. In Figure 8a we show the ratios of the widths of the small-frequency half-profiles (i.e the widths of the left halves of the profiles given the traditional increase of frequency to the right in most plots) to the widths of the large-frequency half-profiles (i.e. the widths of the right halves of the profiles) plotted as a function of frequency. For the case of symmetric peaks this ratio would be equal to one. Inspection of Figure 8a shows that the large majority of the peaks were fit with model profiles which had larger widths on the small-frequency sides of the maxima. In Figure 8b we show the frequency dependence of the frequency differences between the asymmetric and symmetric fits for all of the modes for which we obtained converged solutions with both asymmetric and symmetric model fits. These frequency differences show a very similar frequency variation to that shown earlier in Figure 3a for the differences between the averaged-spectrum and mean-multiplet frequencies which were obtained using the assumption of symmetric profiles in both cases. The amplitude of the frequency variation shown in Figure 8b is about one-half of that shown in Figure 3a and so it is possible that some of the systematic differences shown in Figure 3a are in fact due to the neglect of asymmetry in both frequency estimation methods. If so, then this would seem to imply that the peaks in the m-averaged power spectra are more asymmetric in shape than are the corresponding peaks in the unaveraged spectra. This is an interesting possibility that we are planning to look into shortly. Also, since there is a theoretical explanation for the observed profile shapes, there is also a mathematical function for the asymmetric shapes of the peaks which may be more suitable to use than the asymmetric Lorentzians and Gaussians which we employed in generating Figure 8. We plan to investigate the use of such a theoretical function as a more accurate model of asymmetry in the near future.

3.7. Comparison of Frequency Estimates Computed from Different "Seed" Frequency Sets

Both of the frequency estimation methods which we employed for the tests described in this paper use sets of initial-guess, or so-called "seed," frequencies as input parameters. These sets of "seed" frequencies provide starting points for the two methods which are hopefully close enough to the desired frequencies that the methods will converge to the proper modes rather than to adjacent sidelobes of them,

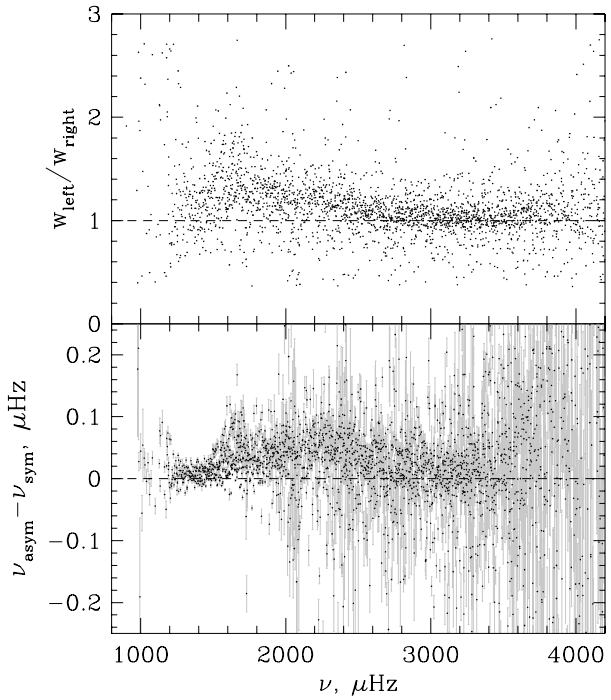

Figure 8. a) Frequency dependence of the ratios of the widths of the left and right halves of the asymmetric profiles used to estimate the amount of asymmetry in the observed power spectral peaks. Symmetric peaks would have ratios equal to unity. Ratios greater than unity correspond to peaks which are wider at smaller frequencies than they are at higher frequencies: b) Frequency dependence of the differences in the frequencies as determined by the averaged-spectrum method using the asymmetric fits and using the assumption of symmetric profiles.

or to noise in the spectra. Specifically, in order for the estimation methods to converge to the proper peaks, these tables of "seed" frequencies must be within a few microhertz of the final solutions for most modes.

Our next test was a test of the sensitivity of our final frequency estimates to changes in our "seed" frequency tables. We carried out this test because the radial profile of the squared differences between the inferred sound speed and our reference solar model which is published by Kosovichev et al. (1997, Figure 12) shows several interesting departures from the reference solar model and we were interested in learning if any of these interesting features could be caused by systematic errors in the "seed" frequencies themselves.

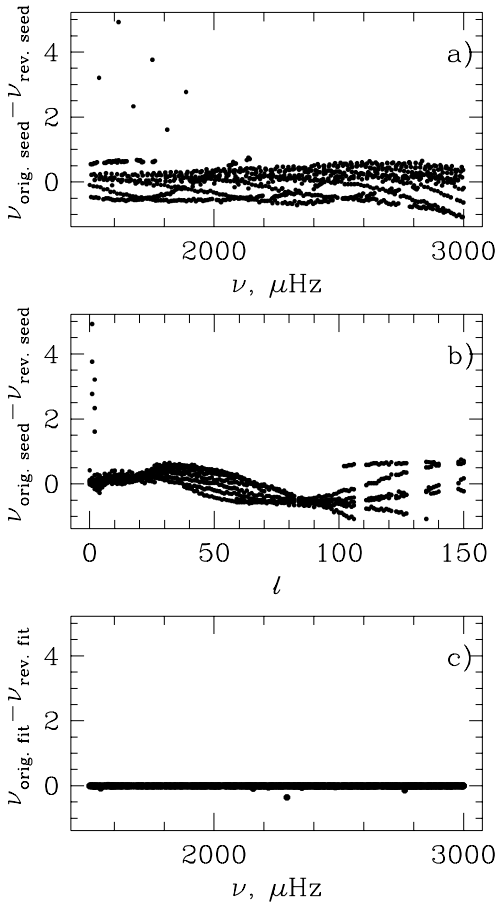

Figure 9. a) Frequency dependence of the differences between the two different sets of "seed" frequencies which were used as inputs to the averaged-spectrum method: b) Degree dependence of the differences in the two sets of seed frequencies: c) Frequency dependence of the differences in the final computed frequencies which resulted from using the two different sets of seed frequencies as inputs to the averaged-spectrum program.

In order to test such a possibility we then conducted a "blind" test in which one of us (AGK) generated a new set of specially-altered "seed" frequencies, after which two others of us (JR and EJR) used this new set of "seed" frequencies as inputs to the averaged-spectrum frequency estimation program. Before showing the results of this test, we wish to illustrate how large the differences in the two sets of "seed" frequencies actually were. The frequency dependence of the differences between the original and the revised "seed" frequencies is shown here in Figure 9a,

while the degree dependence of these same "seed" frequency differences is shown in Figure 9b. Inspection of Figure 9b shows that there was a pronounced degree dependence in the differences in the two sets of "seed" frequencies, with a peak-to-peak amplitude of three microhertz between $l = 30$ and $l = 110$.

Once we had computed the additional set of modal parameter estimates, we compared them with the parameters obtained from the original set of "seed" frequencies. For the frequency estimates of the modes we simply matched up common modes in our two tables and then subtracted the two estimates. The results of this comparison are shown here in Figure 9c. Figure 9c shows the frequency dependence of the differences in the two sets of frequency estimates. A quick glance at this figure shows that, with the exception of a very small number of modes for which the frequency differences ranged between -0.05 and -0.4 microhertz, all of the remaining frequency differences were less than $\pm$ 20 nanohertz. Such tiny frequency differences will have no measurable effects on the sound speed profiles which will be shown in the next section.

4. Inversion Results

4.1. Radial Stratification from Mean-multiplet Frequencies

We have determined the spherically symmetric structure of the Sun by using the optimally localized averaging techniques (Backus and Gilbert, 1968; 1970) to invert three different sets of frequencies, ν_{nl}, obtained from the mean-multiplet method. Figure 10a shows the relative differences between the square of the sound speed in the Sun and model S of Christensen-Dalsgaard *et al.* (1996) for three different sets of mean-multiplet frequencies. The large dots with the superimposed horizontal and vertical error bars are the results of the inversion of the full set of 2047 frequencies obtained from the 144-day observing run. The dashed curve (which is almost indistinguishable from the dots over most of the figure) shows the results of a similar inversion of the subset of those modes which were common to the averaged-spectrum method. This subset contained 1940 modes. (Thiss common-mode subset of the mean-multiplet data set is also included on the CD-ROM for comparison with the full mode set.) The curve comprised of small dots with no errors bars gives the result of an inversion of the set of 1473 modes obtained from the 60-day observing run which was previously published by Kosovichev *et al.* (1997).

It is important to note that the inversion results represents localized estimates of the sound speed, which can be interpreted as a result of convolution of the solar sound-speed profile with localized averaging kernels, a sample of which is shown in Figure 11 (a data file with the kernels is available on the CD-ROM). These kernels are obtained as linear combinations of the sensitivity functions of individual modes with no a priori assumption about the solar sound-speed profile. When the solar

models are compared with the inversion results, the model sound-speed profiles must be convolved with the averaging kernels.

In Figure 10, the inversion results are characterized by four parameters: the localized average of the squared sound-speed difference between the sun and the reference model, the central position of the averaging kernels, the formal error estimate obtained from the errors of the frequencies of the individual modes, and the characteristic width of the kernals ('spread'). For the central position and for the width, we have adopted the definitions by Backus and Gilbert (1968, 1970), which fully account for the sidelobes of the localized kernels and their asymmetry that are particularly important near the center and the surface.

Occasionally, the effects of the sidelobes and asymmetry are ignored in presentations of inversion results when some other definitions for the central location and for the width are employed (e.g. Turck-Chieze et al, 1997; Basu et al, 1996) resulting in a misleading impression of improvement of the resolution of the core structure or the structure of subsurface layers. However, the true resolution can be judge only through examining the averaging kernels, also because quite often an attempt to obtain a more narrow central peak leads to higher sidelobes, in particular, near the surface. Since the subsurface structure is not well determined yet, doing so may result in substantial systematic errors in the localized averages representing the core structure.

All three of these inverted profiles in Figure 10a show that the maximum difference in the square of the sound speed between the model and the Sun is only 0.4%. Nevertheless, this difference is very important for understanding solar evolution and physical processes inside the Sun. One feature that is common to all three of these sound-speed profiles is particularly notable. This is the narrow peak centered at 0.67 R, just beneath the convection zone. This peak was previously detected in the LOWL (Basu *et al.*, 1996) and GONG data (Gough *et al.*, 1996) and is most likely due to a deficit of helium in the sun in comparison with the reference solar model in this narrow region. The deficit of helium decreases the mean molecular weight and thus increases the sound speed. The deficit of helium could result from additional mixing of the material in the layer with the surrounding plasma if turbulence is generated in this layer because of rotational shear. Indeed, as was shown by Kosovichev *et al.* (1997), there is a strong radial gradient of the rotation rate in this layer.

A second interesting feature that is common to all three profiles is the decrease in the sound speed that occurs between 0.30 R and 0.25 R, or just outside the energy-generating core. The three curves begin to deviate from one another inward of 0.25 R. In particular, the two inversions from the 144-day dataset both remain low, while the profile from the 60-day run shows a turn-up toward 0.075 R. The absence of this increase in sound speed toward the solar center in the two 144-day inversions is most likely due to the removal of some low-degree modes which were included in the inversion of the 60-day dataset. Hence, the reality of this turn-up in sound speed inward of the minimum near $0.20R$ must await the accumulation of

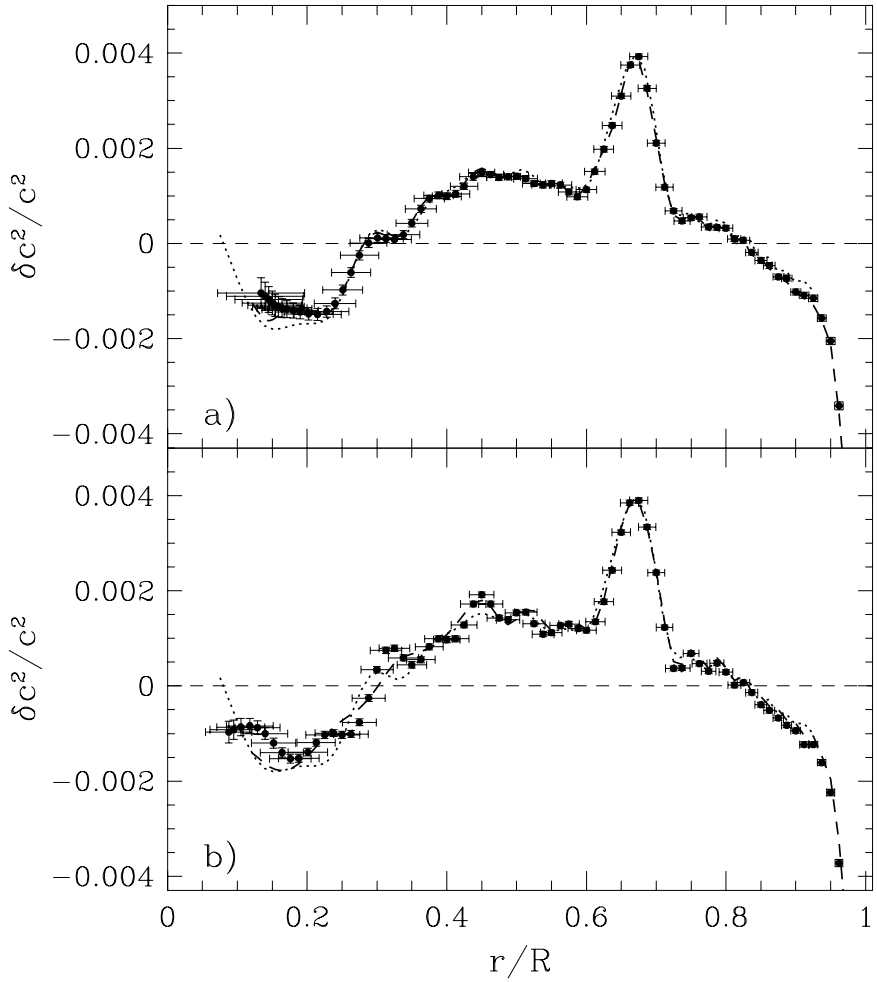

Figure 10. a) Relative differences between the squared sound speed in the Sun and a standard solar model as inferred from three inversions of the frequency estimates computed with the mean-multiplet method from the MDI Medium-l data. The curve comprised of large dots with superimposed error bars came from the inversion of the entire set of 2047 frequencies obtained from the 144-day observing run. The dashed curve came from an inversion of a subset of 1940 of these modes that was common to the mode set determined from the averaged-spectrum method. The curve of small dots came from the inversion of the 1473 frequencies obtained from the 60-day observing run: b) Radial profiles of similar inferred squared sound speed deviations from the standard solar model as inferred from the inversion of the averaged-spectrum frequency estimates. The large dots with the error bars were from from the inversion of the entire 144-day set of 2794 modes. The dashed curve was from the inversion of the set of 1940 modes that was common to the mean-multiplet mode set. The small dotted curve is repeated from the top panel for reference. In both panels the horizontal bars show the spatial resolution of the inferred values, while the vertical bars are the formal error estimates. These inversion results are compared in the color version of this figure on the CD-ROM. The four new sound-speed profiles are also included on the CD-ROM in tabular format.

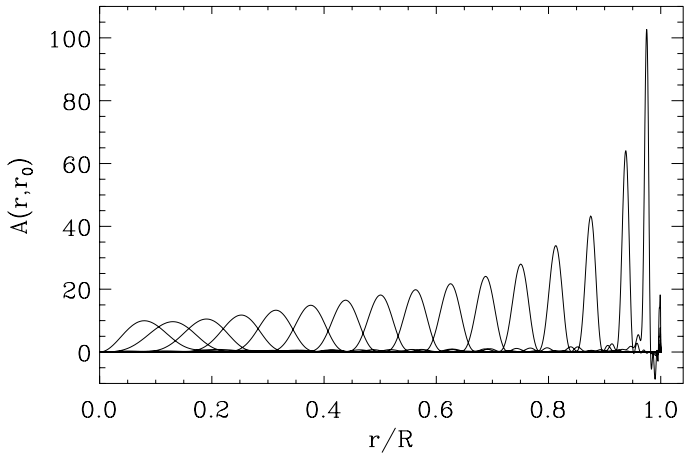

Figure 11. Localized averaging kernels for the squared sound-speed estimates.

additional observations of the low-degree modal frequencies which were removed from the 144-day mean-multiple dataset. These low-degree frequencies were deleted because they did not pass the reliability criteria for the 144-day run (see e.g. Schou, 1992).

4.2. Radial Stratification from Averaged-Spectrum Frequencies

We also obtained additional estimates of the spherically symmetric structure of the solar internal sound speed by using the same inversion techniques, but by applying them to invert the frequency estimates obtained from the averaged-spectrum method. Figure 10b shows the relative differences between the square of the sound speed in the Sun and the same model S of Christensen-Dalsgaard *et al.* (1996) as determined by inversions of the full set of 2794 averaged-spectrum modes (the large dots with the horizontal and vertical errors) and of the 1940 modes common to the mean-multiplet data set (the dashed curve).(This common-mode subset of the averaged-spectrum frequencies is also included on the CD-ROM for comparions with the full mode set.) These two additional estimates of the radial profile of the internal sound speed show several similarities to the profiles shown in Figure 10a. Most importantly, both of these profiles also show the same sharp increase in the square of the sound speed at a radius of 0.67 R which was seen in the radial profiles which resulted from the inversions of the mean-multiplet frequency estimates shown in Figure 10a.

Furthermore, both of these radial profiles of the solar sound speed show evidence for the decrease in the sound speed outside the solar core that is shown in Figure 10a. However, the inverted profile obtained from the full mode set shows more

radial variation in this region than does the profile obtained from the common mode set. Any verification of this extra variation will have to await the acquisition and analysis of additional observations. Also, both averaged-spectrum profiles show that the sound speed reaches a similar minimum value to that found in the mean-multiplet profiles inside of 0.20 R.

Finally, both of the averaged-spectrum profiles show some evidence for the turn-up toward the center that is seen in the Kosovichev *et al.* (1997) 60-day inversion. However, this turn-up is less prominent in the new inversions. Since the inversion results near the center depend only on a few low-degree modes (e.g. Gough, Kosovichev, and Toutain, 1995) that are particularly difficult to measure, the turn-up must be viewed with caution until we obtain more precise measurements of the low-degree mode frequencies.

5. Conclusions

The results of the different numerical tests which we have reported above suggest that we must continue to work diligently in order to learn whether or not the systematic differences in the frequency estimates which we have found are in fact due to the effects of the asymmetry of the observational peaks or whether they are due to another, as yet undetermined, cause. In particular, we must do so before we will be able to have confidence in the entire radial range of the sound speed profile which we have obtained from our current inversion computations. The potential importance of every deviation of the solar sound speed profile from that in our standard reference solar models is so great that we must continue our attempts at finding and learning about all possible sources of systematic errors in the input datasets which will be used as inputs to future inversion investigations. We must also put great effort into determining the validity of the low-frequency and low-degree modal fits which have a large influence on the sound speed in the solar core.

On the other hand, we have also demonstrated that we can anticipate that the formal frequency uncertainties which are employed as additional inputs to the inversion programs will continue to decrease as additional days of observations are included in the time series from which the observational power spectra are computed. This decrease in frequency uncertainties will increase our confidence in the inverted profiles once we have been able to eliminate the systematic errors which still exist.

We have also demonstrated that one of the more interesting features in the radial profile of the solar internal sound speed which has been found in the past few years from both GONG and MDI data, namely the rather narrow peak in the deviation of the sound speed from that of the current reference solar model beneath the convection zone, is not due to either any peculiarity in the choice of the seed frequencies which were employed in the determination of the frequencies

which went into those inversions nor is it due to the particular method of frequency estimation that is employed.

Finally, all five of the inversions we have presented here also show evidence for a similar minimum value in the sound speed relative to the standard solar model in the solar core. The question of whether the sound speed remains low throughout the core or whether it once again increases toward the very center of the sun is a matter that must await the acquisition additional observations to be resolved.

Acknowledgments

The authors acknowledge many years of effort by the engineering and support staff of the MDI development team at the Lockheed Palo Alto Research Laboratory (now Lockheed-Martin) and the SOI development team at Stanford University. SOHO is a project of international cooperation between ESA and NASA. This research is supported by the SOI-MDI NASA contract NAG5-3077 at Stanford University. The portion of this research which was conducted at USC and at the Technical University of Munich was supported by Stanford University Sub-Contract Number PR 6914 to USC and by NASA Grant NAGW-13 to USC. Portions of the computations for this research were carried out using the facilities of USC's Campus Computing Center. J.R. is grateful to R. Bulirsch for his generous support and hospitality.

References

Abrams, D., and Kumar, P.: 1996, *Astrophys. J.*, **472**, 882.
Backus, G. and Gilbert, F. 1968, *Geophys. J. R. astr. Soc.*, **16**, 169.
Backus, G. and Gilbert, F. 1970, *Phil. Trans. R. Soc., A***266**, 123.
Bahcall, J.N., and Pinsonneault, M.H.: 1995, *Rev. Mod. Phys.*, **67**, 781.
Basu, S., Christensen-Dalsgaard, J., Schou, J., Thompson, M.J., and Tomczyk, S.: 1996, *Bull. Astr. Soc. India*, **24**, 147.
Brown, T., private communication, 1996.
Christensen-Dalsgaard, J., Däppen, W., and the GONG Team: 1996, *Science*, **272**, 1286.
Duvall, T.L., Harvey, J.W., and Pomerantz, M.A.: 1986, *Nature*, **321**, 500.
Duvall, T.L., Jr., Jefferies, S.M., Harvey, J.W., Osaki, Y., and Pomerantz, M.A.: 1993, *Astrophys. J.*, **410**, 829.
Gabriel, M.: 1992, *Astron. Astrophys.*, **265**, 771.
Gabriel, M.: 1993, *Astron. Astrophys.*, **274**, 935.
Gabriel, M.: 1995, *Astron. Astrophys.*, **299**, 245.
Gough, D.O.: 1993, in J.P. Zahn and J. Zinn-Justin (eds), *Astrophysical Fluid Dynamics*, Elsevier, Amsterdam, p. 399.
Gough, D.O., Kosovichev, A.G., and Toutain, T.: 1995, *Solar Phys.*, **157**, 1.
Gough, D.O., Kosovichev, A.G., and the GONG Team: 1996, *Science*, **272**, 1296.
Hill, F., Stark, P.B., Stebbins, R.T., and the GONG Team: 1996, *Science*, **272**, 1292.
Korzennik, S.G.: 1990, Ph.D. Dissertation, Univ. Calif. Los Angeles.
Kosovichev,A.G.,Schou, J., Scherrer, P.H., Bogart, R.S., Bush, R.I., Hoeksema, J.T., Aloise, J., Bacon, L., Burnette, A., De Forest, C., Giles, P.M., Nigam, R., Rubin. R., Basu, S.,

Christensen-Dalsgaard, J., Dappen, W., Rhodes, E.J., Jr., Duvall, T.L., Jr., Howe, R., Thompson, M.J., Gough, D.O., Sekii, T., Toomre, J., Tarbell, T.D., Title, A.M., Mathur, D., Morrison, M., Wolfson, C.J., and Zayer, I.:1997, *Solar Phys.*, in press.

Kumar, P., Fardal, M.A., Jefferies, S.M., Duvall, T.L., Jr., Harvey, J.W., and Pomerantz, M.A.: 1994, *Astrophys. J.*, **422**, L29.

Nigam, R., and Kosovichev, A.G.: 1996, in J. Provost and F.X. Schmider (eds), *Sounding Solar and Stellar Interiors*, Proc. IAU Symp. 181, Nice, France, 30 Sept.- 3 Oct., 1996, Kluwer Acad. Publ., in press.

Reiter, J. and Rhodes, E.J.,Jr.:1997, SOI Technical Note, in preparation.

Ritzwoller, M.H. and Lavely, E.M.: 1991, *Astrophys. J.*, **369**, 557.

Rogers, F.J., and Iglesias, C.A.: 1996, *Astrophys. J.*, **456**, 902.

Roxbourgh, I.W., and Vorontsov, S.V.: 1995, *Monthly Notices Roy. Astron. Soc.*, **272**, 850.

Scherrer, P.H., Bogart, R.S., Bush, R.I., Hoeksema, J.T., Kosovichev, A.G., Schou, J., Rosenberg, W., Springer, L., Tarbell, T.D., Title, A., Wolfson, C.J., Zayer, I., and the MDI Engineering Team: 1996, *Solar Phys.*, **162**, 129.

Schou, J.: 1992, *On the Analysis of Helioseismic Data*, Thesis, Aarhus University .

Turck-Chieze, S., Basu, S., Brun, S., Christensen-Dalsgaard, J., Eff-Darwich, A., Lopes, I., Perez Hernandes, F., Berthomieu, G., Provost, J., Ulrich, R.K., Baudin, F., Boumier, P., Charra, J., Gabrial, A.H., Garcia, R.A., Grec, G., Renaud, C., Robillot, J.M., and Roca Cortes, T.: 1997, *Solar Phys.*, submitted